



## Research Article

# pH dependent ZnO nanostructures synthesized by hydrothermal approach and surface sensitivity of their photoelectrochemical behavior

Kaoruho Sakata<sup>1</sup>  · Kateřina Minhová Macounová<sup>1</sup> · Roman Nebel<sup>1</sup> · Petr Krtil<sup>1</sup>

Received: 22 October 2019 / Accepted: 6 January 2020 / Published online: 13 January 2020  
© Springer Nature Switzerland AG 2020

## Abstract

Nanoparticulate ZnO materials were fabricated using microwave assisted hydrothermal synthesis from mixture of zinc acetate and ammonia at variable pH. The particle size and shape of resulting materials changes with the pH of precursor solution. The obtained nanoparticulate ZnO are of single phase nature with particle size ranging between 100 and 3000 nm, and are photoelectrochemically active in water oxidation upon UV illumination. Their photoelectrochemical activity, depends primarily on the ZnO particle surface orientation which changes with the particle size. The highest photoelectrochemical activity results from simultaneous presence of {0–110} and {–2110} oriented faces. The presence of {0001} oriented faces apparently suppresses the photoelectrochemical activity. The results indicate that the photoelectrochemical activity of ZnO is mainly related to a presence of {0–110} oriented surface.

**Keywords** ZnO · Nanoparticle · Hydrothermal synthesis · Photoelectrochemistry · Surface sensitivity

## 1 Introduction

Zinc oxide (ZnO) is wurtzite-type crystal structure material and one of the most studied wide band gap n-semiconductors ( $E_g = 3.37$  eV) mainly due to numerous applications [1, 2]. ZnO is also low cost and environmental friendly hence it can be naturally used in various practical applications, i.e. photocatalysis [3, 4], sensors [5, 6], solar cells [7] and optical devices [8]. Photocatalytic properties of ZnO are of great interest and consequently they have been extensively studied. Especially, photocatalytic water splitting for hydrogen generation is one of the most important applications in the photocatalysis field [9–14]. The ZnO properties are often compared with those of TiO<sub>2</sub> due to similarity in bandgap and band edge positions. In contrast to TiO<sub>2</sub>, it is expected that ZnO will allow for easier scale up needed for development of a large area water

splitting platforms due to lower cost and better environmental friendliness.

Various fabrication methods have been reported for ZnO nanostructures and nanoparticles including, e.g. hydrothermal and solvothermal syntheses [4, 14–19], thermal decomposition [20, 21], sol–gel method [22] and chemical vapor deposition [13]. The hydrothermal synthesis can make crystals with narrow size distribution and high purity, including particles of various shape, even in absence of additives. This should be very useful because the particle morphology can be tuned according to its final application. As for microwave assisted hydrothermal synthesis, it can shorten the reaction time compared with conventional hydrothermal systems, which lowers the energy consumption. Microwave assisted hydrothermal synthesis has been reported not only for ZnO [23] but also for various materials syntheses, e.g.  $\alpha$ -Fe<sub>2</sub>O<sub>3</sub>, CuO and TiO<sub>2</sub> [15]. Although shaping the ZnO nanocrystals in the

✉ Kaoruho Sakata, kaoruho.sakata@jh-inst.cas.cz | <sup>1</sup>J. Heyrovský Institute of Physical Chemistry, Academy of Sciences of the Czech Republic, Dolejškova 3, 18223 Prague, Czech Republic.



hydrothermal preparation has been reported [17, 24–26], there is lack of understanding of the surface sensitivity in photoelectrochemical activity of ZnO nanocrystals. Despite the availability of the single crystal focused studies targeting the photoelectrochemical behavior of ZnO [27, 28] these data cannot be directly transferred to the nanostructure materials due to possible synergetic effect resulting from coexistence of different surface orientations at the nanocrystal surface.

In this study, the microwave assisted additive free hydrothermal synthesis was used to fabricate nanostructures/nanoparticles of different sizes and shapes from mixture of zinc acetate and ammonium solution at variable pH. The relationship between the surface sensitivity of photoelectrochemical activity associated with crystal size/shape in water oxidation was investigated.

## 2 Experimental

### 2.1 Synthesis

The samples of the ZnO nanoparticles were synthesized by microwave assisted hydrothermal method using SpeedWave IV system (Berghof). For the synthesis,  $\text{Zn}(\text{CH}_3\text{COO})_2 \cdot 2\text{H}_2\text{O}$  (ACS grade, Wako Chemicals),  $\text{NH}_4\text{OH}$  hydroxide (25%, Aldrich) were used. First 0.1 M zinc acetate solution was prepared by dissolving  $\text{Zn}(\text{CH}_3\text{COO})_2 \cdot 2\text{H}_2\text{O}$  in Milli-Q quality water. Then 12 ml of 0.1 M zinc acetate solution and 0.25, 0.5, 1.0, 1.5, 2.0 or 3.0 ml of  $\text{NH}_4\text{OH}$  (25%) was put into the reaction vessel, and Milli-Q quality water was added to the mixture until total volume became 24 ml. The hydrothermal synthesis was carried out at 150 °C for 30 min. Following the synthesis, the resulting precipitate in the reaction vessel was filtered, washed with Milli-Q quality water, and dried at 150 °C for 2 h.

### 2.2 Characterization

Crystallinity and phase purity was checked by X-ray diffraction (XRD) using powder X-ray diffractometer (Rigaku Miniflex) with Cu K $\alpha$  radiation. Scanning electron microscopy (SEM) characterization was carried out using a S4800 system (Hitachi) and obtained secondary electrons (SE) images. The band gap of the synthesized samples was determined by UV–Vis diffuse reflectance spectroscopy (DRS) (PerkinElmer LAMBDA 950).

Photoelectrochemical activity of the prepared materials in water oxidation was tested in a three electrode arrangement with ZnO working, Pt auxiliary and Ag/AgCl reference electrodes. In the result and discussion, the all measured potentials were recalculated and are presented in a reversible hydrogen electrode (RHE) scale.

Photoelectrochemical experiments were carried out in chronoamperometric mode using AUTOLAB (PGSTAT 30) potentiostat for potential control. The potential dependence of the photoelectrochemical activity was constructed from individual chronoamperometric experiments. All photoelectrochemical measurements were repeated three times and presented values were obtained by averaging.

The ZnO electrodes were prepared on fluorine-doped tin oxide (FTO) glass (TEC 15, Dyesol, 15  $\Omega$ /sq), by drop-casting approach. The initial ZnO suspension was prepared by dispersing 5 mg of ZnO along with 1.4 mg of polyethylene glycol (PEG) 2000 (Aldrich) in 0.2 ml of Milli-Q quality water. The ZnO layer on FTO was deposited by dropping 10  $\mu\text{l}$  increments of the ZnO based suspension which were subsequently dried at 400 °C. The weight of the ZnO deposit on the substrate was measured by weighing the substrate before and after each deposition. The photoelectrochemical experiments were performed under monochromatic illumination using the Bluepoint LED spot source (Hönle UV Technology) with the 365 nm wavelength, an intensity of 6 W/cm<sup>2</sup> as an illumination source. The measurements were performed in  $\text{N}_2$  purged 0.1 M  $\text{Na}_2\text{SO}_4$  aqueous solution.

## 3 Results and discussion

### 3.1 Crystal structure of ZnO nanoparticles

The structure of the synthesized ZnO materials reflected in XRD conforms to that ZnO (see Fig. 1) as shows its comparison with the literature data of ZnO (ICSD # 82028). The observed XRD patterns are not affected by the pH at which the synthesis was performed. The positions of all observed diffraction peaks can be indexed as the hexagonal ZnO.

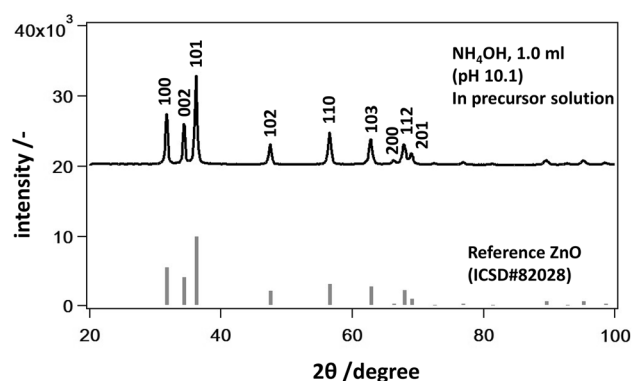


**Fig. 1** The XRD pattern of ZnO nanoparticles prepared by microwave assisted hydrothermal synthesis at 150 °C, 30 min, with the amount of  $\text{NH}_4\text{OH}$  of 1.0 ml (pH 10.1) in the precursors as mineralizer. Reference data of ZnO is from ICSD #82028

Relatively narrow diffraction peaks imply that ZnO is well crystallized. The lattice parameters and the density of each ZnO material evaluated from the XRD patterns are shown in Table 1. The obtained lattice constants show a minor variation with the synthetic conditions. The biggest deviation in lattice constant is observed for the ZnO synthesized with addition of 1 ml of  $\text{NH}_4\text{OH}$  (pH of 10), however, even in this case the observed deviation does not exceed  $2\delta$ .

### 3.2 Relationship between pH of precursor and morphology of particles

The variation of the ammonium hydroxide amount in the reaction mixture has a pronounced effect on the reaction yield and on the shape of the prepared ZnO materials as well. The dependence of the reaction yield on the initial pH of the reaction mixture is shown in Fig. 2. The variation of the reaction yield is statistically insignificant as long as the pH remains in the 9–11 interval. The yield initially increases with increasing pH; reaches its maximum at pH of 10 but decreases at more alkaline pH values. The observed pH dependence of yield results from a confluence of two effects. First of all, increase of pH increases the kinetics of the Zn(II) acetate hydrolysis which is prerequisite for ZnO crystallization. The increasing extent of hydrolysis increases the crystallization rate of ZnO which reaches its maximum at pH 10. Further increase in reaction mixture alkalinity, however, does not bring higher crystallization rate due to a stabilization of  $\text{ZnO}_2^{2-}$  anions in the solution which decreases the supersaturation driving the crystallization process.

The change of actual supersaturation reflects itself also in the size and shape of the ZnO crystals obtained in hydrothermal synthesis starting at different pH. As shows Fig. 3, the hydrothermal synthesis at pH of 7 yields rather bulk micrometer sized individual crystal with characteristic hexagonally shaped prismatic part capped with truncated pyramids. The width of the prismatic part cross-section is approximately  $1\ \mu\text{m}$  while the length of the crystals is approximately  $5\ \mu\text{m}$ . Materials grown hydrothermally at higher pH in the range 8–10 are significantly smaller in the sub-micron range and reach the smallest particle size of ca. 100 nm in the material prepared at initial pH of 10.

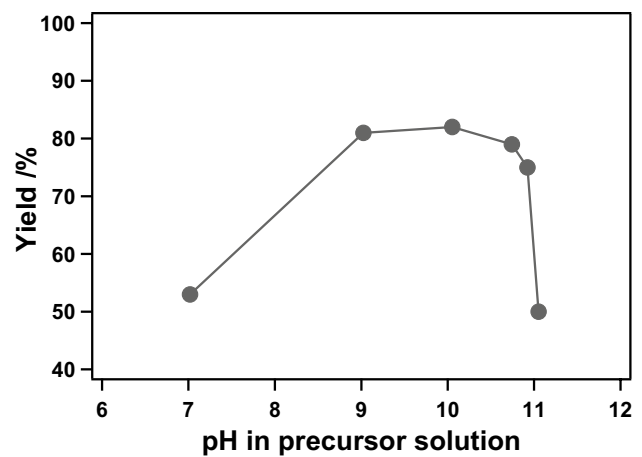


Fig. 2 The dependence of the reaction yield on the initial pH of the reaction mixture

The crystals grown under these conditions show a similar elongated shape as the ones prepared at pH of 7. In contrast, however, the crystal faces seem to be less developed than on the crystals grown at pH 7. In fact a closer examination reveals the observed crystals to consist of finer nanoparticles which apparently coalesce together via Ostwald ripening. It needs to be noted that the decrease of the particle size is accompanied with a significant increase in the yield. It may be, therefore, assumed that the increase of the yield is caused by an increased supersaturation which primarily affects nucleation of smaller crystallites and the growth of which is hindered. An increase of the pH of synthetic mixture close to 11 leads to a formation of a flower-like crystallite agglomerates when elongated crystals similar to those obtained at pH of 7 start to form. The flower-like arrangements are formed by a micron sized crystals which at a closer inspection still reveal smaller crystallites (ca. 100–2000 nm) assembled to form elongated large particles. The trend to form large crystals continues also in the materials synthesized at pH higher than 11.

The increased pH, however, brings up higher tendency to dissolution of the primary precipitated nuclei and subsequent slower growth. This is accompanied with gradual decrease of the yield of the synthesis (see Fig. 2). It also leads to a formation of relatively smooth crystal faces

**Table 1** The lattice parameters and the density of each ZnO nanoparticles sample derived from the XRD spectrum

Amount of $\text{NH}_4\text{OH}$ in precursor solution (ml)	0.25	0.5	1	1.5	2	3	Average ( $\pm 2\delta$ )
pH in precursor solution	7.0	9.0	10.1	10.7	10.9	11.1	
Lattice a, b (Å)	3.255	3.254	3.259	3.253	3.254	3.255	3.255 ( $\pm 0.004$ )
Lattice c (Å)	5.212	5.209	5.218	5.213	5.215	5.215	5.215 ( $\pm 0.006$ )
Density ( $\text{g cm}^{-3}$ )	5.654	5.659	5.633	5.658	5.652	5.648	5.651 ( $\pm 0.019$ )

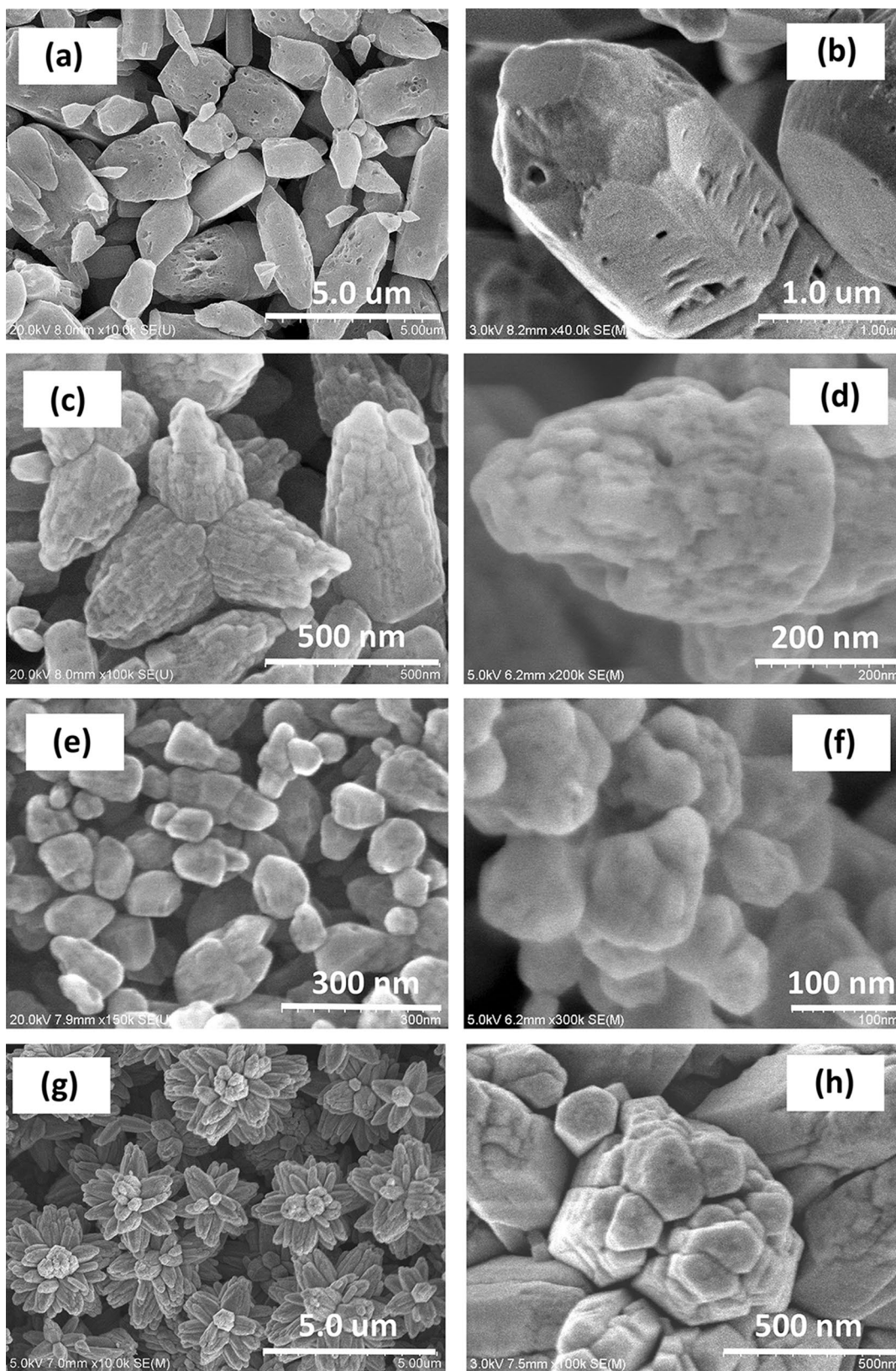


**Fig. 3** SEM images of ZnO **a, b** for pH 7.0 in precursor solution, **c, d** for pH 9.0, **e, f** for pH 10.1, **g, h** for pH 10.7, **i, j** for pH 10.9 and **k, l** for pH 11.1 added to zinc acetate aqueous solution as precursor for

the syntheses. All figures are secondary electrons (SE) images. For more precise observation on the sample surface, the SEM images with higher magnification are shown on **(b), (d), (f), (h), (j)** and **(l)**

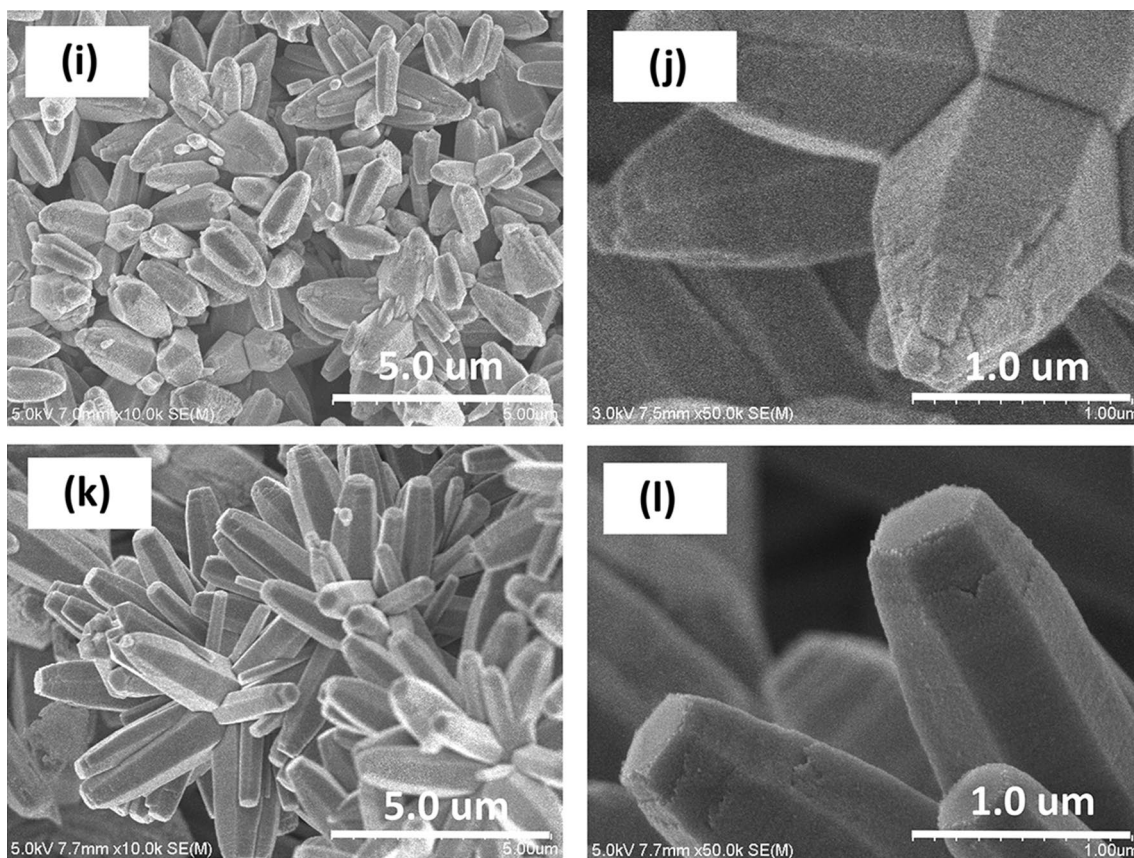


Fig. 3 (continued)

which form a hexagonal prismatic part capped with two hexagonal pyramids. It needs to be noted that in contrast to material synthesized at pH 7 these pyramidal faces are not truncated. Further increase of the pH of the reaction mixture causes faster growth of individual crystals which still seem to grow from single vertices. Further growth, however, leads to crystals with higher aspect ratio (3:1 in contrast to 2:1 observed for all other materials). The increase in pH also leads to a truncation of the capping pyramids clearly exposing well developed  $\{0001\}$  faces.

With respect to the wurtzite structure of the prepared ZnO one can assume there are three preferential growth directions: along the z-axis (i.e.  $\{0001\}$ ); along the  $\{-2110\}$  and along  $\{0-110\}$  vectors [1]. The elongated shape of the crystals along with a dominating presence of the hexagonal cross-section is observed in all well developed crystals which is compliant with the preferential growth of the crystals in the  $\{0001\}$  direction. Such a growth would naturally expose the  $\{0-110\}$  oriented faces on the surface of the pyramidal parts of the deposited crystals. One can relate the hexagonal faces similarly, truncating the capping pyramids to the high stability  $\{0001\}$  faces.

It needs to be noted that  $\{0001\}$  oriented faces can be found only in materials the crystallization of which is controlled by growth, i.e. which either grow from relatively low number of nuclei or which have the chance to optimize its shape by dissolution/reprecipitation mechanism.

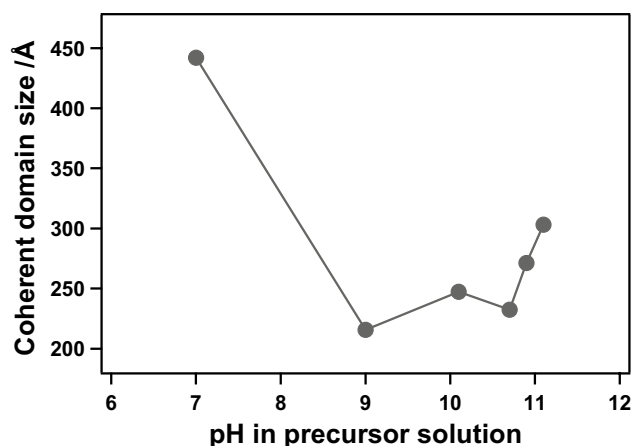


Fig. 4 Coherent domain size of ZnO particles derived by Scherrer equation from XRD spectrum

The suggested mechanism seems to be supported also by coherent domain size data (see Fig. 4) which show the smallest value for materials lacking {0001} facets and also by aspect ratio of the prepared crystals (see Fig. 5b).

Regardless of the difference in particle and coherent domain sizes prepared ZnO samples show identical band gap energy as show UV-Vis spectra (see Fig. 6). Such a behavior can be expected since the particle size of all prepared material is significantly larger than anticipated Debye length in ZnO (ca. 10 nm) [29].

### 3.3 Photoelectrochemical experiments

All prepared materials are photoelectrochemically active and one can observe an anodic photocurrent at bias values higher than 0.18 V vs. RHE (as shown in Fig. 7a). The photocurrent vs. bias dependence shows a typical sigmoidal shape reflecting the formation of the space charge layer. The observed photocurrent increases with increasing bias until the bias reaches ca. 0.7 V vs. RHE. At higher biases one

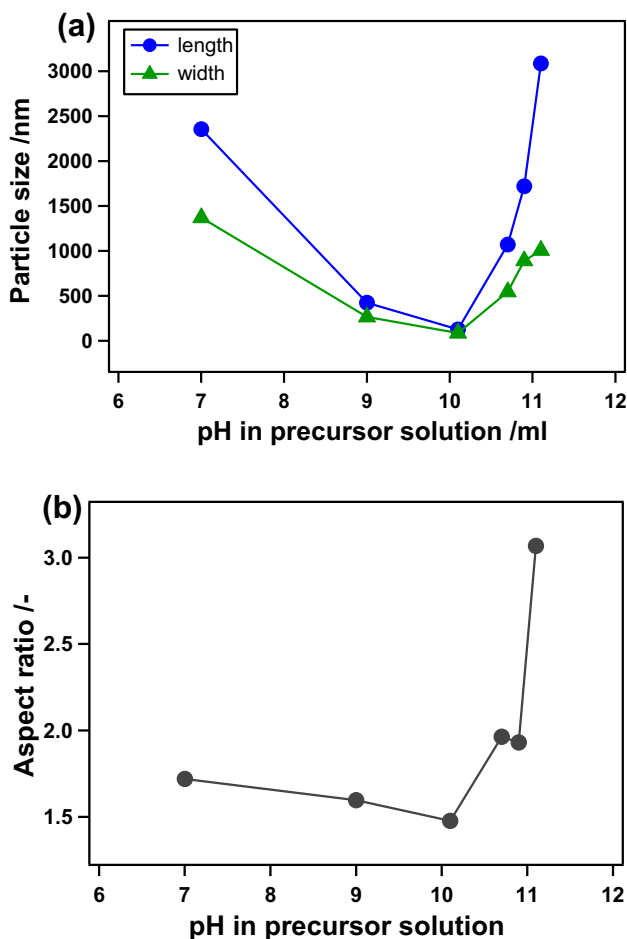


Fig. 5 **a** The length and width of the ZnO nanoparticles estimated from SEM images and **b** their aspect ratio

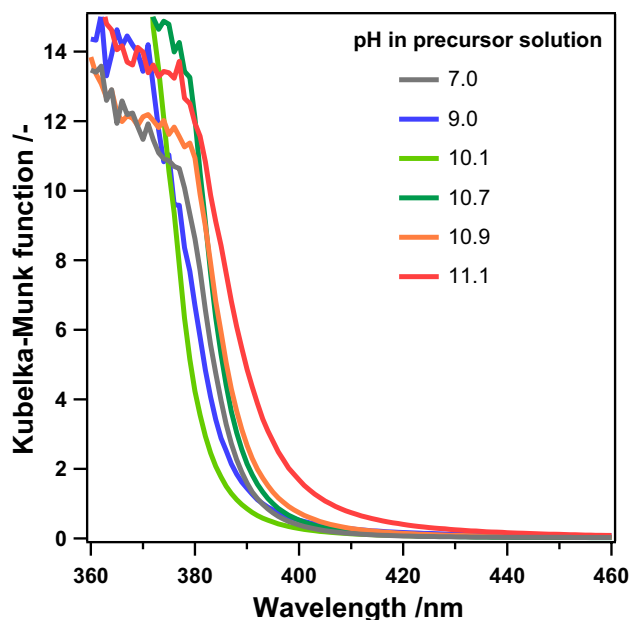
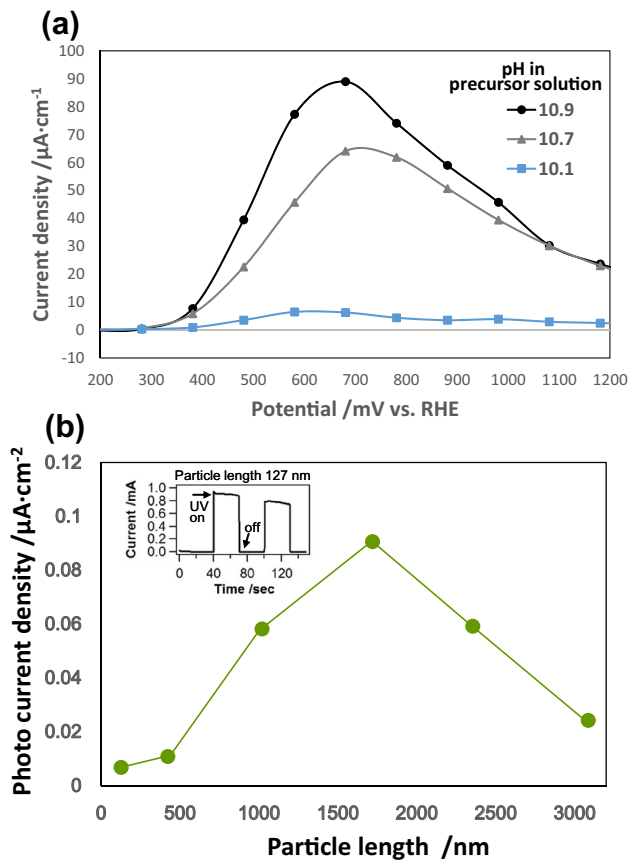


Fig. 6 UV-Vis spectra of ZnO nanoparticles

observes a slight decrease of the measured photocurrent. Such a behaviour is to be expected due to the n-type semi-conducting nature of the ZnO. Given the position of the valence and conduction band one can assign the observed anodic photocurrent to oxygen evolution via water oxidation. The bias needed to drive measureable photocurrent does not change for materials synthesized at different conditions. The limiting photocurrent density recorded at bias higher than 0.58 V vs. RHE, however, depends on the particle size (see Fig. 7b). In contrast to intuitive expectation the photocurrent density reflecting the activity of ZnO crystals in photoelectrochemical water oxidation changes with characteristic particle size. Such a behaviour is rather counterintuitive. It also needs to be noted that the activity of the flower-like ZnO exceeds that of the isolated particles despite possible problems with absorption of the UV exciting radiation one may expect for flower-like materials.

This unusual behaviour can be rationalized keeping in mind the prevailing orientation of the surface one obtains at the surface of individual crystals composing the prepared electrodes. It needs to be noted, that the lowest activity was received for materials featuring the smallest crystals, which also show smallest degree of surface orientation. The activity of ZnO remains low also in materials featuring slightly increased particle size ( $d \sim 500$  nm) due their tendency for Ostwald ripening growth, which still fails to form well defined faces at the particle surface.

Significant improvement of the photoelectrochemical activity is, however, encountered in materials which start to feature well developed hexagonal prismatic part of the



**Fig. 7** **a** Photocurrent density of ZnO corresponding to the applied potential V vs. RHE in an aqueous solution of 0.1 M Na<sub>2</sub>SO<sub>4</sub>, under irradiation of UV with the 365 nm wavelength. In this figure, the photocurrent of ZnO nanoparticles with 10.1, 10.7 and 10.9 of pH in precursor solution was chosen as representative data. **b** Photo-current density of ZnO in each size loaded on FTO substrate, and measured at 680 mV vs. RHE. The measured current value was divided by the surface area estimated from SEM images. Also, the current density was for 1 cm<sup>2</sup> of the surface area of electrode

ZnO crystals. These prismatic faces most likely of {0–110} orientation can be deemed as the primary faces for the water oxidation on ZnO. It needs to be noted that highest activity for water oxidation is observed for materials which do not feature {0001} faces, which apparently can play a little role in the photoelectrochemical activity of ZnO.

The photoelectrochemical activity of individual ZnO orientations has been reported before [27, 28, 30]. Zhang et al. [27] suggested the electrode with {0001} orientation terminated with Zn rich facet have lower photocurrent than the {10–10} orientation, on the other hand, the electrode with {0001} orientation (i.e. O-rich) has higher activity compared with the other two. The difference is assigned to a difference in electric fields developed in space charge layer. This has been contradicted by Kislov et al. [28] who ranked the photoelectrochemical activities of ZnO single crystals in the order of (10–10) > (0001) > (000–1),

where ZnO(0001) and ZnO(000–1) represent the Zn- and O-terminated surfaces of this polar material, respectively. Similarly the difference in surface orientation has been reflected also in the experiments of photochemical deposition of Au on ZnO nanorods [30]. It needs to be noted that the results reported in this study are in general agreement with those reported in [28] when the appearance of the {0001} oriented faces in general leads to a drop in photoelectrochemical activity.

## 4 Conclusions

Hydrothermal synthesis is convenient technique capable to grow ZnO crystal of different functionality. The primary variable affecting the photoelectrochemical behavior of ZnO materials is the pH of the starting solution. The crystallization of the ZnO is controlled by the hydrolysis of the Zn acetate at one hand and nucleation and subsequent growth of ZnO from solution on the other. A slow growth from small number of nuclei experienced in neutral media yielding large crystals with well-developed {0–110} and {0001} facets changes into one dominated by a fast nucleation at pH ranging between 8 and 10. Even these materials may grow larger particles via Ostwald ripening. These particles are, however, lacking well defined crystal faces. Further increase of pH leads to a growth of well-defined crystals arranged in flower-like arrangements. The photoelectrochemical activity of the ZnO materials in water oxidation improves with improved crystallinity of the individual ZnO crystals. The presence of well-developed {0–110} faces is pre-requisite for significant photoelectrochemical activity. The development of the well resolved {0001} faces, on the other hand, has a retarding effect on the photoelectrochemical activity. This clearly outlines that the ZnO materials for photoelectrochemical applications need to be developed with maximization on {0–110} faces in mind. This in turn allows for rational selection of the reaction conditions of the ZnO synthesis.

**Funding** This study was funded by the Grant Agency of the Czech Republic (Grant Number 17-128005).

## Compliance with ethical standards

**Conflict of interest** On behalf of all authors, the corresponding author states that there is no conflict of interest.

## References

1. Wang ZL (2004) Zinc oxide nanostructures: growth, properties and applications. *J Phys Condens Matter* 16:R829–R858

2. Özgür Ü, Alivov YI, Liu C, Teke A, Reshchikov MA, Doğan S, Avrutin V, Cho SJ, Morkoç H (2005) A comprehensive review of ZnO materials and devices. *J Appl Phys* 98:041301
3. Tian ZR, Voigt JA, Liu J, McKenzie B, McDermott MJ, Rodriguez MA, Konishi H, Xu H (2003) Complex and oriented ZnO nanostructures. *Nat Mater* 2:821–826
4. Wang AJ, Liao QC, Feng JJ, Zhang PP, Lia AQ, Wang JJ (2012) Apple pectin-mediated green synthesis of hollow double-caged peanut-like ZnO hierarchical superstructures and photocatalytic applications. *Cryst Eng Commun* 14:256–263
5. Mitra P, Chatterjee AP, Maiti HS (1998) ZnO thin film sensor. *Mater Lett* 35:33–38
6. Wang X, Summers CJ, Wang ZL (2004) Large-scale hexagonal-patterned growth of aligned ZnO nanorods for nano-optoelectronics and nanosensor arrays. *Nano Lett* 4:423–426
7. Zhang Q, Dandeneau CS, Zhou X, Cao G (2009) ZnO nanostructures for dye-sensitized solar cells. *Adv Mater* 21:4087–4108
8. Look DC (2001) Recent advances in ZnO materials and devices. *Mater Sci Eng B* 80:383–387
9. Allami S, Ali ZDA, Li Y, Hamody H, Jawad BH, Liu L, Li T (2017) Photoelectrochemical performance of N-doped ZnO branched nanowire photoanodes. *Heliyon* 3:e00423
10. Šulčiūtė A, Ostachavičiūtė S, Valatka E (2017) Synthesis, structure and photoelectrochemical behavior of ZnO coatings on AISI 304 type steel. *Chemija* 28:85–92
11. Wang M, Ren F, Zhou J, Cai G, Cai L, Hu Y, Wang D, Liu Y, Guo L, Shen S (2015) N doping to ZnO nanorods for photoelectrochemical water splitting under visible light: engineered impurity distribution and terraced band structure. *Sci Rep* 5:12925
12. Wang B, Li R, Zhang Z, Wang X, Wu X, Cheng G, Zheng R (2018) An overlapping ZnO nanowire photoanode for photoelectrochemical water splitting. *Catal Today* 321–322:100–106
13. Fang KM, Wang ZZ, Zhang M, Wang AJ, Meng ZY, Feng JJ (2013) Gelatin-assisted hydrothermal synthesis of single crystalline zinc oxide nanostars and their photocatalytic properties. *J Colloid Interface Sci* 402:68–74
14. Wang J, Wang Z, Huang B, Ma Y, Liu Y, Qin X, Zhang X, Dai Y (2012) Oxygen vacancy induced band-gap narrowing and enhanced visible light photocatalytic activity of ZnO. *ACS Appl Mater Interfaces* 4:4024–4030
15. Meng L, Wang B, Ma M, Lin K (2016) The progress of microwave-assisted hydrothermal method in the synthesis of functional nanomaterials. *Mater Today Chem* 1–2:63–83
16. Liu Y, Gao W (2015) Growth process, crystal size and alignment of ZnO nanorods synthesized under neutral and acid conditions. *J Alloys Compd* 629:84–91
17. Demoisson F, Piolet R, Bernard F (2014) Hydrothermal synthesis of ZnO crystals from Zn(OH)<sub>2</sub> metastable phases at room to supercritical conditions. *Cryst Growth Des* 14:5388–5396
18. Søndergaard M, Bøjesen ED, Christensen M, Iversen BB (2011) Size and morphology dependence of ZnO nanoparticles synthesized by a fast continuous flow hydrothermal method. *Cryst Growth Des* 11:4027–4033
19. Baruah S, Dutta J (2009) Hydrothermal growth of ZnO nanostructures. *Sci Technol Adv Mater* 10:013001
20. Andelman T, Gong Y, Polking M, Yin M, Kuskovsky I, Neumark G, O'Brien S (2005) Morphological control and photoluminescence of zinc oxide nanocrystals. *J Phys Chem B* 109:14314–14318
21. McLaren A, Valdes-Solis T, Li G, Tsang SC (2009) Shape and size effects of ZnO nanocrystals on photocatalytic activity. *J Am Chem Soc* 131:12540–12541
22. Meulenkamp EA (1998) Synthesis and growth of ZnO nanoparticles. *J Phys Chem B* 102:5566–5572
23. Wojnarowicz J, Opalinska A, Chudoba T, Gierlotka S, Mukhovskiy R, Pietrzykowska E, Sobczak K, Lojkowski W (2016) Effect of water content in ethylene glycol solvent on the size of ZnO nanoparticles prepared using microwave solvothermal synthesis. *J Nanomater* 2789871
24. Zhang H, Yang D, Ma X, Ji Y, Xu J, Que D (2004) Synthesis of flower-like ZnO nanostructures by an organic-free hydrothermal process. *Nanotechnology* 15:622–626
25. Feng Y, Feng N, Wei Y, Zhang G (2014) An in situ gelatin-assisted hydrothermal synthesis of ZnO-reduced graphene oxide composites with enhanced photocatalytic performance under ultraviolet and visible light. *RSC Adv* 4:7933–7943
26. Sun J, Dong S, Wang Y, Sun S (2009) Preparation and photocatalytic property of a novel dumbbell-shaped ZnO microcrystal photocatalyst. *J Hazard Mater* 172:1520–1526
27. Zheng B, Wang Z, Huang B, Zhang X, Qin X, Li H, Dai Y, Li Y (2016) Anisotropic photoelectrochemical (PEC) performances of ZnO single-crystalline photoanode: effect of internal electrostatic fields on the separation of photogenerated charge carriers during PEC water splitting. *Chem Mater* 28:6613–6620
28. Kislov N, Lahiri J, Verma H, Goswami DY, Stefanakos E, Batzill M (2009) Photocatalytic degradation of methyl orange over single crystalline ZnO: orientation dependence of photoactivity and photostability of ZnO. *Langmuir* 25:3310–3315
29. Hongsith N, Wongrat E, Kerdcharoen T, Choopun S (2010) Sensor response formula for sensor based on ZnO nanostructures. *Sens Actuators B* 144:67–72
30. Read CG, Steinmiller E, Choi K (2009) Atomic plane-selective deposition of gold nanoparticles on metal oxide crystals exploiting preferential adsorption of additives. *J Am Chem Soc* 131:12040–12041

**Publisher's Note** Springer Nature remains neutral with regard to jurisdictional claims in published maps and institutional affiliations.